The perinucleolar compartment and the oncogenic super-enhancers are part of the same phase-separated structure filled with phosphatidylinositol 4,5bisphosphate and long noncoding RNA HANR

Ana Miladinović [a,1], Ludovica Antiga [a,1], Tomáš Venit [a], Andrea Bayona-Hernandez [a,b], Jakub Červenka [c,d], Rajendra Kumar Labala [e], Michal Kolář [e], Enrique Castaño [a,b], Martin Sztacho [a,f,*], Pavel Hozak [a,**]

[a] Department of Biology of the Cell Nucleus, Institute of Molecular Genetics of the Czech Academy of Sciences, Prague, Czech Republic
[b] Unidad de Biología Integrativa, Centro de Investigación Científica de Yucatán, Calle 43, Número 130, Chuburná de Hidalgo, Mérida, Yucatán, CP 97205, Mexico
[c] Laboratory of Proteomics, Institute of Biochemistry and Experimental Oncology, First Faculty of Medicine, Charles University, Prague, Czech Republic
[d] Laboratory of Applied Proteome Analyses, Research Center PIGMOD, Institute of Animal Physiology and Genetics of the Czech Academy of Sciences, Libechov, Czech Republic
[e] Laboratory of Genomics and Bioinformatics, Institute of Molecular Genetics of the Czech Academy of Sciences, Prague, Czech Republic
[f] Laboratory of Cancer Cell Architecture, Institute of Biochemistry and Experimental Oncology, First Faculty of Medicine, Charles University, Prague, Czech Republic

ARTICLE INFO

ABSTRACT

The liquid-liquid phase separation in the cell nucleus regulates various processes such as gene regulation and transcription control, chromatin organization, and DNA repair. A plethora of proteins and RNAs contribute to the formation of biomolecular condensates and recently, several nuclear phosphoinositides were shown to be a part of these membrane-less complexes within the nucleus as well. Here we lipid-interacting RNA sequencing (LIPRNAseq) and confocal microscopy to uncover the RNA-binding capacity and localization of phosphatidylinositol 4,5 bisphosphate (PIP2). We discovered the consensus PIP2-binding AU-rich RNA motif and identified long non-coding RNA HANR (lncHANR) to colocalize with PIP2 in the proximity to the nucleolus in the perinucleolar compartment (PNC). Colocalization studies with different nuclear markers reveal that PIP2-HANR presence in the PNC correlates with oncogenic super-enhancers, and both PNC and oncogenic enhancers are part of the same structure. As lncHANR, PNC, and oncogenic super-enhancers are associated with cancer cell lines and tumors, we suggest that they can serve as interchangeable prognostic markers. Understanding of the interplay between lipid metabolism,

* Corresponding author. Laboratory of Cancer Cell Architecture, Institute of Biochemistry and Experimental Oncology, First Faculty of Medicine, Charles University, Prague, Czech Republic.
** Corresponding author. Department of Biology of the Cell Nucleus, Institute of Molecular Genetics of the Czech Academy of Sciences, Prague, Czech Republic.
E-mail addresses: martin.sztacho@lf1.cuni.cz (M. Sztacho), hozak@img.cas.cz (P. Hozak).
[1] These authors contributed equally.

and lncRNAs in subnuclear compartment phase separation can lead to future improvement in treatment strategies and personalized cancer management approaches.

1. Introduction

Transcriptional dysregulation in cancer involves the abnormal control of gene expression, where oncogenes are overactivated and/or tumor suppressor genes are silenced or repressed. This is often driven by mutations in transcription factors, epigenetic modifications, or changes in chromatin structure that alter cell signaling pathways. As a result, cancer cells can bypass growth controls, modulate their metabolism, proliferate uncontrollably, and resist cell senescence. Initial studies were focused on understanding single gene mutations in cancer development and were followed by the understanding of local epigenetic modulations and chromatin rearrangements during carcinogenesis. More recently, gradual attention has been given to cis-regulatory long-range chromatin interactions, 3D chromosome organization, and compartmentalization of the cell nucleus and their role in cancer development and progression (Adeel et al., 2021; Eidelman et al., 2017; Kim et al., 2022; Tang et al., 2015; Casalin et al., 2024; Owusu Obeng et al., 2020; Ratti et al., 2021). Super-enhancers, as an example of such regulatory element, are large clusters of enhancers driving the expression of cell fate-determining transcription factors during differentiation (Whyte et al., 2013; Hnisz et al., 2013; Villar et al., 2015). However, when hijacked by cancer cells, they can regulate the robust expression of oncogenes. These oncogenic super-enhancers are hallmarks of cancer and are associated with bad survival prognosis (Bacabac et al., 2023a; Liu et al., 2024; Debek et al., 2022; Jia et al., 2020). The landscape of oncogenic super-enhancers in cancer is characterized by high levels of histone H3K27 acetylation and high concentration of Bromodomain-containing protein 4 (BRD4), and Mediator complex as well as several other chromatin remodelers, transcription factors, and transcription activators (Bacabac et al., 2023a). The proteins surrounding the super-enhancers form biomolecular condensates, which are membrane-less compartments formed through liquid-liquid phase separation of proteins and nucleic acids to provide local microenvironments for various cellular functions, including transcription regulation (Sabari et al., 2018; Hnisz et al., 2017; Boija et al., 2018). Mediator of RNA polymerase II transcription subunit 1 (MED1) and Bromodomain containing 4 protein (BRD4) were shown to have a substantial role in the phase separation due to their intrinsically disordered regions facilitating condensation at oncogenic super-enhancers. This separation of phases allows for a local increase in the concentration of transcription factors and RNA polymerase II, thus promoting robust transcription of surrounding genes (Sabari et al., 2018; Tong et al., 2022).

Phosphoinositides are a class of phospholipids known to play roles in both cytoplasm and the nucleus. In the cytoplasm, as a part of the plasma membrane, they are responsible for the transduction of signals, vesicular trafficking, and others (Casalin et al., 2024; Posor et al., 2022; Wen et al., 2023; Castano et al., 2019). Several phosphoinositides have also been found in the cell nucleus, but their function is still poorly understood. Phosphatidylinositol 4,5 bisphosphate (PIP2) is distributed throughout the nucleoplasm and clusters in the nucleoli, nuclear speckles, and unique structures previously identified as nuclear lipid islets (NLIs) (Sobol et al., 2018; Hoboth et al., 2021, 2023, 2024). Depending on the interacting partners, PIP2 was shown to have a role in numerous biological processes, with regulation of RNA Polymerase I and II transcription, regulation of chromatin remodeling, and mRNA processing to be the most described (Balaban et al., 2021, 2023; Lewis et al., 2011; Sztacho et al., 2021). It has been suggested that PIP2 functions in the cell nucleus by sequestering its interaction partners into phase-separated condensates (Sztacho et al., 2019). The presence of phospholipids, particularly PIP2, within these nuclear condensates, has been shown to contribute to their stability and functionality (Sobol et al., 2018; Balaban et al., 2023). NLIs are thought to facilitate the formation of these condensates by providing a favorable environment and a platform for multivalent interactions of proteins involved in transcription. Recent studies have reported that phosphoinositides are particularly enriched within MED1 biomolecular condensates where they affect their shape (Dumelie et al., 2024). This aligns with our recent data, demonstrating that PIP2 pulls down MED1 and BRD4 from nuclear protein extracts, indicating that PIP2 is an integral component of MED1/BRD4 phase-separated structures (Sztacho et al., 2024).

Moreover, PIP2 has been shown to interact with different RNAs and the RNase treatment of semi-permeabilized cells leads to the dissociation of NLIs in the cell nuclei (Sobol et al., 2018; Bayona-Hernandez et al., 2023). This agrees with the literature, as nucleic acids, and particularly RNA, are essential for the formation of phase-separated structures in the cell nucleus. Furthermore, long non-coding RNAs (lncRNAs) play a crucial role in gene regulation and nuclear architecture within the nucleus. lncRNAs can promote the assembly of transcriptional condensates by providing a structural framework that facilitates the interaction between various transcriptional regulators (Luo et al., 2021; Somasundaram et al., 2022). This spatial organization is crucial for effective gene expression and cellular responses to environmental stimuli. Apart from their direct role in gene regulation, lncRNAs contribute to the nuclear architecture and spatiotemporal regulation of processes by encouraging phase separation. Through their secondary structure, lncRNAs serve as architectural scaffolds, thus enabling local enrichment of proteins and lipids to enhance the formation of different nuclear bodies (Mao et al., 2010; Shevtsov et al., 2011). For example, paraspeckles are membrane-less structures in the cell nucleus that are condensed around scaffold lncRNA *NEAT1* (Luo et al., 2021; Somasundaram et al., 2022; Hirose et al., 2014, 2019; Pisani et al., 2019; Shadrina et al., 2022; Wang et al., 2020). Similarly, in the perinucleolar compartment (PNC), which is a dynamic subnuclear structure located at the periphery of the nucleolus, lncRNA *PNCTR* sequesters Polypyrimidine tract-binding protein 1 (PTBP1) to inhibit its splicing regulatory function, thereby modulating alternative splicing events in the nucleoplasm (Yap et al., 2018). Taken together, the capacity of phosphoinositides and lncRNAs to mutually interact and modify the physical state of nuclear compartments underscores the complexity of phase separation mechanisms in the nucleus, integrating lipid metabolism and RNA biology into the regulatory networks governing gene expression, and suggests their potential involvement in disease mechanisms, such as cancer

progression (Sztacho et al., 2024; Lin et al., 2017; Li et al., 2021; Frankowski et al., 2022).

Therefore, in our current study, we focused on PIP2-RNA interactions *in vivo* and uncovered their spatial distribution within the cell nucleus. We showed that PIP2 has an affinity to AU-rich RNA motifs within lncRNAs which have a role in genome organization, ribonucleoprotein complex biogenesis, and mRNA splicing. Depending on the RNA motif, the PIP2-RNA complex localizes to distinct nuclear compartments associated with either Pol II transcription or mRNA splicing. Most importantly, we showed that the localization of oncogenic super-enhancers fully correlates with the localization of the PNC, suggesting that they are part of the same phase-separated structure containing PIP2-RNA complexes. Finally, we have discovered hepatocellular carcinoma associated long non-coding RNA (HANR), a lncRNA associated with several types of cancer and their progression (Xiao et al., 2017; Xu et al., 2020), to be localized in the PNC/super-enhancers phase-separated region together with PIP2.

2. Results

2.1. PIP2-associated RNAs have a role in genome organization, chromosome segregation, and mRNA processing

The PIP2-bound RNAs were identified by the lipid-interacting RNA sequencing (LIPRNAseq) method described previously (Bayona-Hernandez et al., 2023). The method is based on *in vitro* pulldown of nuclear RNAs with the PIP2-bound agarose beads and subsequent sequencing which led to the discovery of 813 differentially expressed transcripts (DETs) that were significantly (fold change >10) overrepresented in PIP2-bound bead samples in comparison to empty beads (negative control). We focused on lncRNAs as they are the most abundant RNA species in the nucleus and were shown to have a role in the phase separation of nuclear processes (Ayupe et al., 2015; Tong et al., 2021; Zaghlool et al., 2021). These PIP2-bound RNAs were subsequently used for gene set enrichment analysis (GSEA) to identify the specific biological processes or nuclear compartments associated with PIP2-RNA complexes. While the statistical significance is relatively low for all GSEA terms due to the elusive biological relevance of the majority of known lncRNAs (Derrien et al., 2012; Iyer et al., 2015) and their general underrepresentation in GSEA, we were able to identify several biological processes associated with the genome organization, chromosome dynamics, and posttranscriptional mRNA processing to be enriched (Fig. 1A). This agrees with cellular component GSEA terms, which are also associated with the chromosomal regions, ribonucleo-protein granules, and spliceosomal complexes (Fig. 1B).

2.2. PIP2 preferentially binds to AU-rich RNAs

Next, we focused on the identification of RNA motifs that bind to PIP2 and their verification *in vivo*. We used MEME Suite (Version 5.4.1) for motif enrichment analysis and identified 38 significant motifs in PIP2-bound RNAs, and two motifs with longer sequences were selected for further analysis. While both sequences are AU-rich, they differ in GC content. Motif AU1 (AUGUAAAAAAAAAAUUAAAGAAAAAAAAAAAAAAUAAAAA) contains a low percentage of GC content within its sequence (5%), while motif AU2 (UUUUUCAAGAGUGAUAAAAAGUUUUUGGCCC) contains higher GC content (31%) compared to the AU1 motif. To test whether these RNA motifs are present in PIP2-containing structures *in vivo*, we used RNA *in situ* hybridization (RNA-ISH) paired with indirect immunofluorescence labeling of PIP2 in the U2OS cells (Fig. 2A and B). Both reverse complementary probes show various and dispersed labeling in the nucleoplasm, with the AU1 RNA motif colocalizing into multiple foci together with PIP2 (Fig. 2A). In
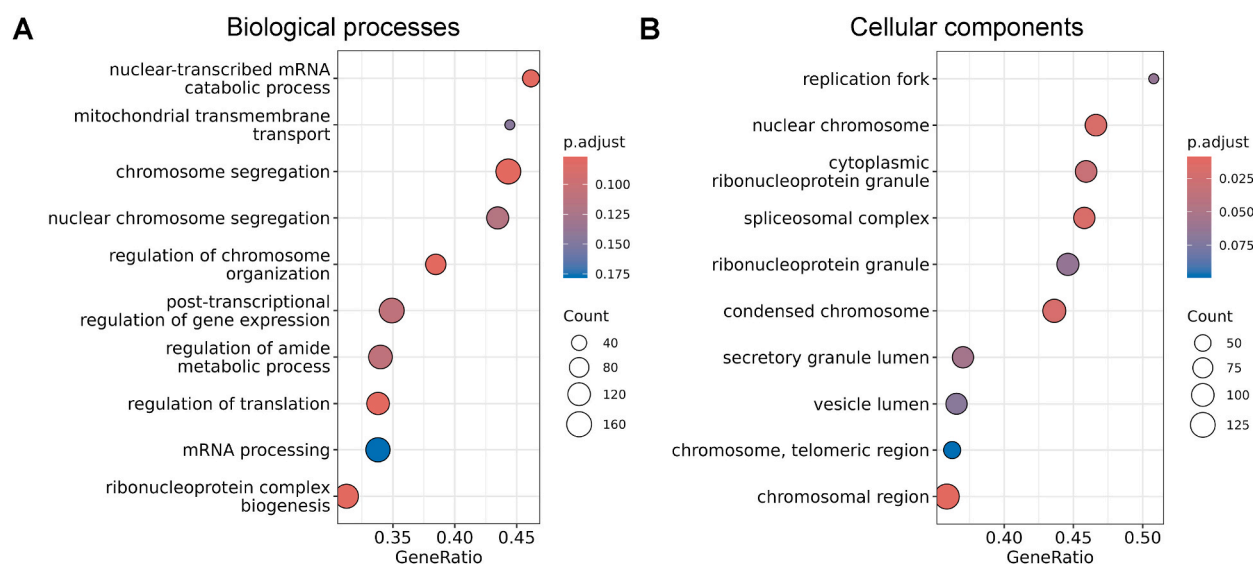

Fig. 1. *GSEA of differentially expressed genes identified by LIPRNAseq.* Plots represent the distribution of analyzed differentially expressed genes across biological processes (A) and cellular components (B) gene ontology terms.

contrast, the AU2 RNA motif predominantly localizes with PIP2 in an isolated spot (Fig. 2B), suggesting that the nuclear localization of different RNAs with PIP2 depends on their sequence. To test this, we used a control FISH probe consisting of only GCs and two AU-rich probes with the same nucleotide content as AU1 and AU2 motifs but with the scrambled sequence (Supplementary Fig. 1). None of the control probes displayed any specific enrichment within the PIP2-containing structures, indicating that the nuclear localization of particular RNAs with PIP2 is dependent on both - the overall AU content and the sequence order.

2.3. PIP2-RNA complexes are enriched in nuclear speckles and perinucleolar compartment

To define RNA-PIP2-containing structures in more detail and to get insights into the possible function of these complexes, we next assess the colocalization of both RNA motifs with various nuclear markers. As PIP2 predominantly colocalizes with nuclear speckles, we first performed RNA-ISH with both probes in cells stained with the speckle-specific marker, SON protein. In agreement with previous results, the probe recognizing the AU1 RNA motif colocalizes with SON protein in nuclear speckles (Fig. 3A). The AU2 RNA motif exhibits cluster-like signal enrichment within one of the nuclear speckles marked by the SON protein (Fig. 3B). Interestingly, while AU1 RNA motif localization in nuclear speckles is observed in all cells, the AU2 RNA motif accumulates to a single visible SON-positive nuclear speckle in only about 20% of cells. This suggests that PIP2-bound AU2-specific RNA is spatially different from AU1 suggesting different functions within the cell nucleus.

Therefore, we further focused on the peculiar localization of the AU2 RNA motif. We performed immunofluorescent staining of markers for selected membrane-less phase-separated structures - nucleoli, nuclear speckles, Cajal bodies, PML bodies, paraspeckles, and PNC. We coupled it to the RNA ISH with a probe against the AU2 RNA motif (Fig. 4). The AU2 RNA motif clusters around the nucleolus stained by anti-Fibrillarin antibodies (Fig. 4A), and colocalize with the PNC stained by anti-hnRNPI antibody (Fig. 4B). Interestingly, the AU2 RNA motif seems to be partially colocalizing with paraspeckle marker SFPQ (Fig. 4C), and in proximity to PML bodies (Fig. 4D). Cajal body marker Coilin does not show colocalization with an AU2-rich cluster in the cell nucleus (Fig. 4E).

2.4. The perinucleolar compartment functions as an oncogenic super-enhancers

The PNC has been associated with Pol III transcription and mRNA processing due to the abundance of Pol III RNA transcripts and several RNA-binding proteins (Pollock et al., 2010; Makeyev et al., 2024; Norton et al., 2013). However, its assembly close to the nucleolus seems to be dependent on specific DNA locus (Norton et al., 2009), suggesting that the higher-order organization of the genome is implicated in the development of PNC. As both, PIP2 and several lncRNAs were shown to contribute to chromatin landscape, and PIP2 is associated with the *Pol*I and Pol II transcription, we hypothesized that the PIP2-AU2 RNA complex could have a role in transcription-dependent chromatin organization within PNC. Enhancers are an example of higher-order genomic structures serving as cis-regulatory elements to regulate the transcription of specific genes. The oncogenic super-enhancers are large clusters of transcriptional enhancers that recruit high levels of chromatin remodelers, transcription factors, transcription activators, and Mediator complexes into specific foci, which results in the overexpression of genes crucial for maintaining the malignant state of the cell (Blayney et al., 2023; Wang et al., 2019; Das et al., 2023; Jia et al., 2019). Therefore, we confirmed colocalization of AU2-rich PNC with the MYO1C, a general transcription factor, and chromatin remodeler associated with all three polymerases (Cavellan et al., 2006; Obrdlik et al., 2010; Percipalle et al., 2006; Philimonenko et al., 2004; Pestic-Dragovich et al., 2000) (Fig. 5A); a mediator complex component MED1 (Fig. 5B); and clustering with the transcriptional activator BRD4 (Fig. 5C). The MED1 and BRD4 were previously
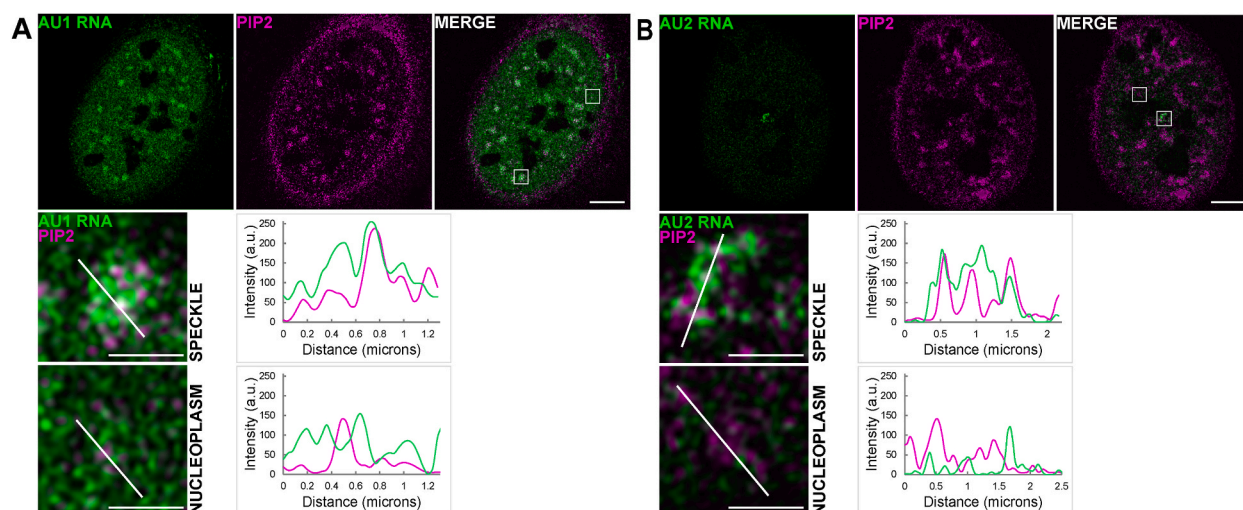
Fig. 2. *Immunofluorescent staining of the PIP2-binding RNA motifs coupled with PIP2 staining.* Both AU1 (A) and AU2 (B) motifs colocalize with PIP2 in nuclear speckles (upper inset and line scan) while they seldom overlap with nucleoplasmic PIP2 signal (lower inset and line scan). The scale bar represents 5 μm in the main images and 1 μm for the insets.
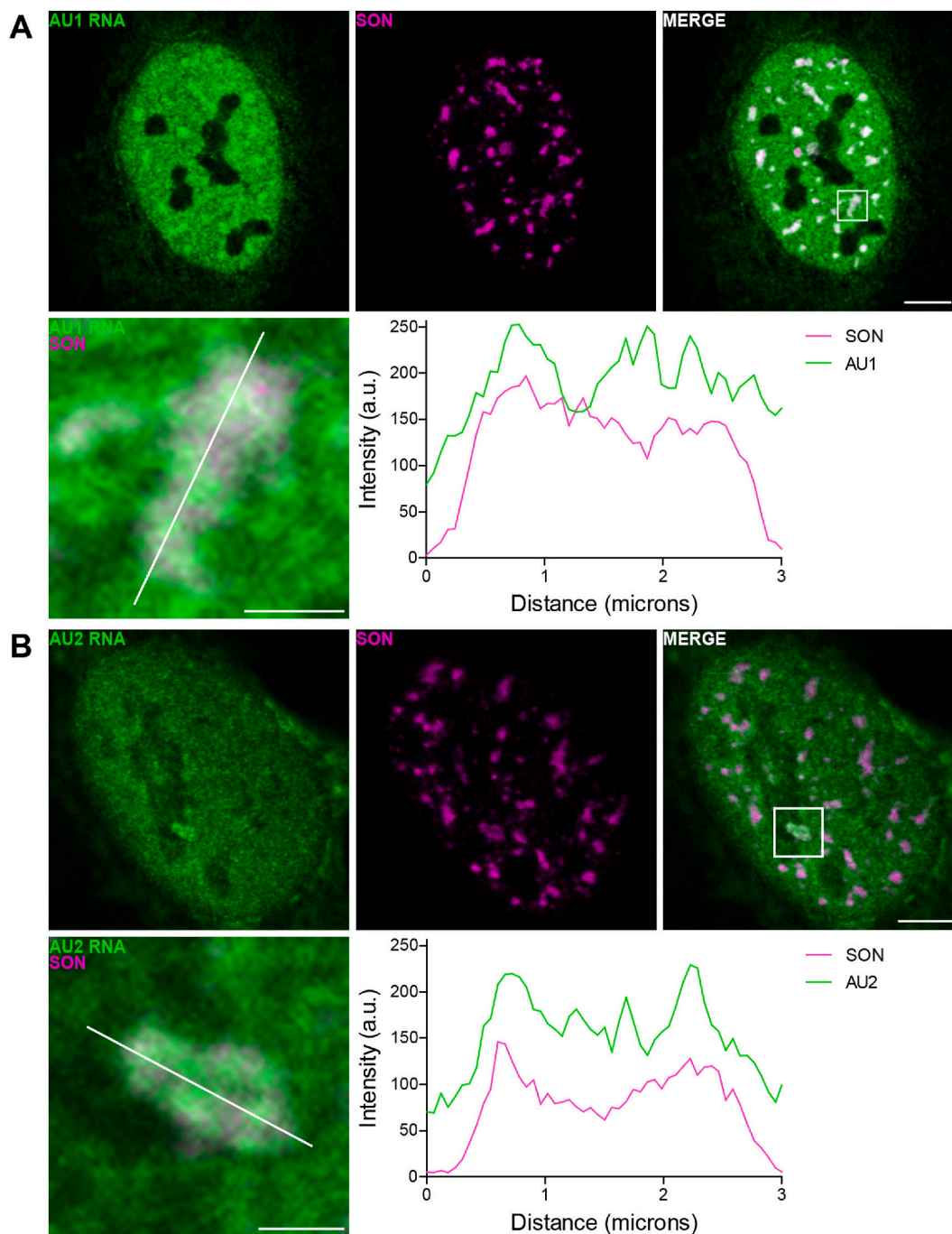
Fig. 3. *Immunofluorescent staining of the PIP2-binding RNA motifs coupled with immunostaining of nuclear speckle marker SON*. The PIP2 RNA motifs AU1 (A) and AU2 (B) display strong nuclear staining where they colocalize with the signal of nuclear speckle marker protein SON. The scale bar represents 5 μm in the main images and 1 μm for the insets.

shown to be present at oncogenic super-enhancers (Bacabac et al., 2023b) and both are associated with PIP2 (Sztacho et al., 2021). Moreover, AU2 RNA colocalizes with DNA damage foci marker 53BP1 (Fig. 5D) and homologous recombination protein RAD51 (Fig. 5E) as physiological double-strand breaks and RAD51 are enriched at highly active oncogenic super-enhancers (Hazan et al., 2019). Thus, PIP2-AU2 RNA complex colocalizes in PNC with MYO1C and MED1, as well as with 53BP1 and RAD51, while BRD4 forms clusters in close vicinity to the PIP2-AU2 RNA complex. Similarly to BRD4, *PolI*, and Pol II surround the PIP2-AU2 RNA cluster but do not colocalize with it directly (Fig. 5F and G, respectively).
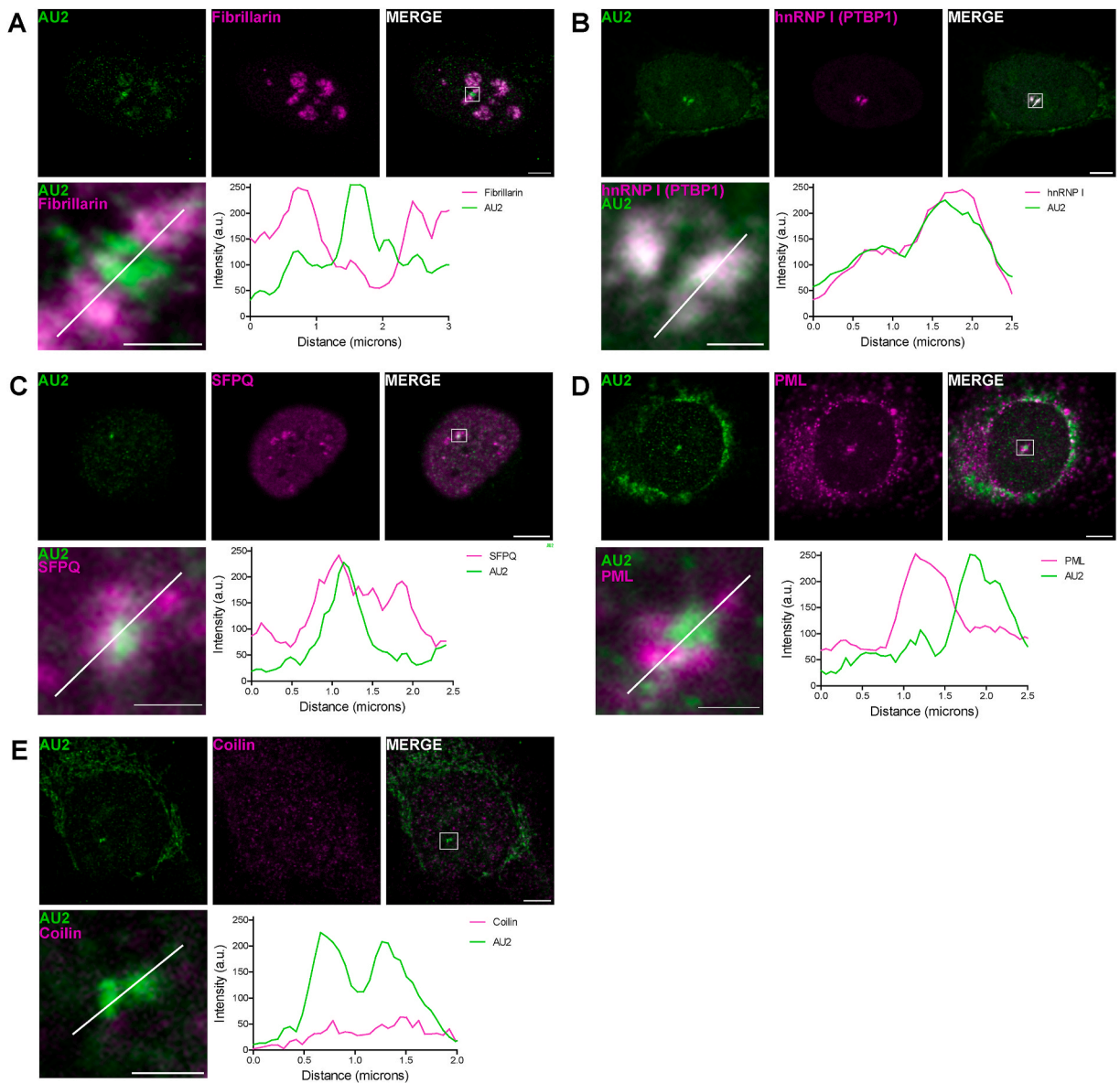
Fig. 4. *Immunofluorescent staining of the AU2-rich motif with different markers of nuclear structures.* AU2-rich structures are shown in the green channel and Fibrillarin (A), hnRNP I (B), SFPQ (C), PML bodies (D), and Coilin (E) in the magenta channel. The scale bar represents 5 μm in the main images for all merged channels and 1 μm for the insets. (For interpretation of the references to colour in this figure legend, the reader is referred to the Web version of this article.)

2.5. PIP2 interacts in the perinucleolar compartment with long-noncoding RNA HANR

We showed that the probe recognizing the AU2 RNA motif colocalizes into the PNC together with PIP2. However, this motif is only a consensus sequence discovered by *in silico* analysis of all PIP2-bound RNAs and does not represent actual RNA. Thus, we wanted to identify the endogenous lncRNA recognized by the AU2 RNA probe, which forms a complex with PIP2 in PNC. Therefore, we employed LIPRNAseq of PIP2-bound RNA, and subsequently performed global sequence alignment of identified lncRNAs with the AU2 RNA motif described previously.

This analysis led to the discovery of lncRNA HANR, which has been reported to be overexpressed in several types of cancers (Xiao et al., 2017; Xu et al., 2020). The sequence alignment analysis of AU1 and AU2 motifs with lncRNA HANR shows that while the AU1 motif is not found in the lncRNA HANR sequence, the AU2 motif sequence partially overlaps with the HANR sequence in the AU-rich region (Fig. 6A).

As PIP2 was shown to bind AU-rich sequences, we next prepared a specific probe for the lncRNA HANR which does not overlap with the AU2-recognized region to avoid unspecific binding with PIP2. *In situ* hybridization with the HANR probe followed by confocal
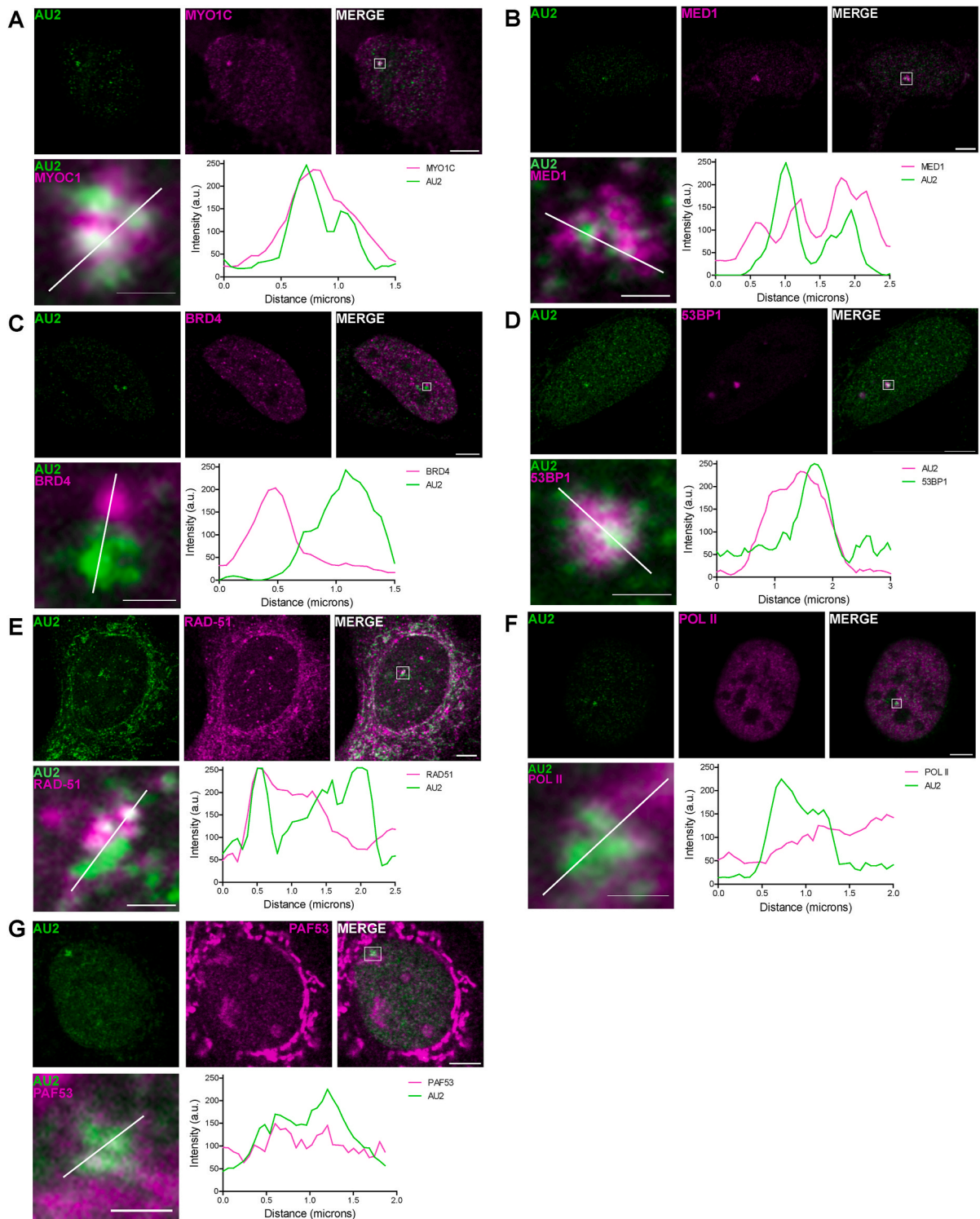
Fig. 5. *Immunofluorescent staining of the AU2-rich motif with different nuclear proteins.* AU2-rich structures are shown in the green channel and MYO1C (A), MED1 (B), BRD4 (C), 53BP1 (D), RAD51 (E), POL II (F) and POLI subunit, PAF53 (G) in magenta. The scale bar represents 5 μm in the main images for all merged channels and 1 μm for the insets. (For interpretation of the references to colour in this figure legend, the reader is referred to the Web version of this article.)
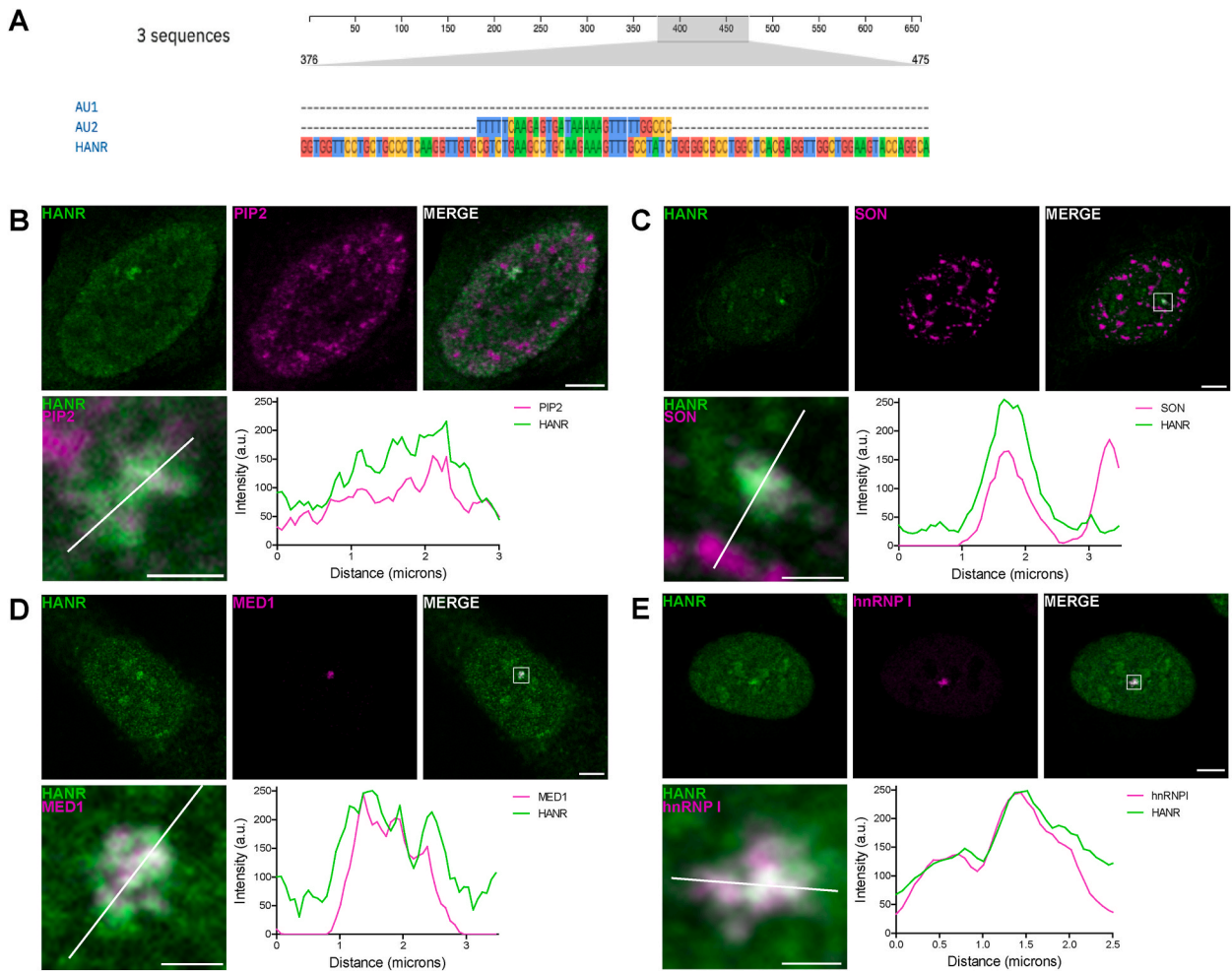
Fig. 6. *lncRNA HANR is localized in PNC and oncogenic super-enhancers together with PIP2.* (A) Sequence alignment between AU1 and AU2 consensus motifs and lncRNA HANR. (B–E) Indirect immunostaining detecting lncRNA HANR is shown in a green channel with PIP2 (B), with speckle marker protein SON (C), with transcription coactivator MED1 (D), and with perinuclear marker, hnRNP I (E) in the magenta channel. The scale bar represents 5 μm in the main images for all merged channels and 1 μm for the insets. (For interpretation of the references to colour in this figure legend, the reader is referred to the Web version of this article.)

microscopy shows that lncRNA HANR is present in proximity to the nucleolus, colocalizing with PIP2 (Fig. 6B), SON (Fig. 6C), MED1 (Fig. 6D), and hnRNPI (Fig. 6E) in the same way as we show for AU2 RNA motif (Figs. 4 and 5). As PIP2 has been shown to support the phase-separation of compartments, we were next interested in whether manipulation with PIP2 levels would affect the localization or total amount of lncRNA HANR in the cell nucleus. As nuclear PIPs can be metabolized inside the nucleus thanks to the presence of all the metabolic enzymes required for their production (Castano et al., 2019), we modulated the PIP2 levels by knocking down specific enzymes through siRNAs. The selected enzymes were PIP5KA1 and SHIP2; the first is kinase, which adds a second phosphate group to PI4P to generate PIP2. In contrast, the second one, SHIP2, is the phosphatase that dephosphorylates the PIP2 and PIP3 at the 5-position of the inositol head group, yielding PI4P and PI(3,4)P2, respectively (Deleris et al., 2003). As a result, the knockdown (KD) of PIP5KA1 leads to a decrease in nuclear PIP2 levels, while in SHIP2 KD, nuclear PIP2 levels are elevated (Lundquist et al., 2018). Overall, the results of RNA ISH coupled with immunofluorescent staining show that manipulation of PIP2 levels does not affect the localization of the lncRNA HANR in the PNC. However, the nucleoplasmic portion of lncRNA HANR seems to be affected and upregulation of PIP2 leads to scattered localization of lncRNA HANR into multiple smaller foci (Fig. 7A), which is further proved by RT-qPCR showing that the overall level of lncRNA HANR increases with the increasing levels of PIP2 (Fig. 7B).

Collectively, our findings reveal that the PNC, previously associated only with *Pol*I and III transcription and RNA processing, may function as an oncogenic super-enhancers. Additionally, we identify PIP2 in complex with the lncRNA HANR as structural components of the PNC, likely contributing to the phase separation of oncogenic genomic loci.
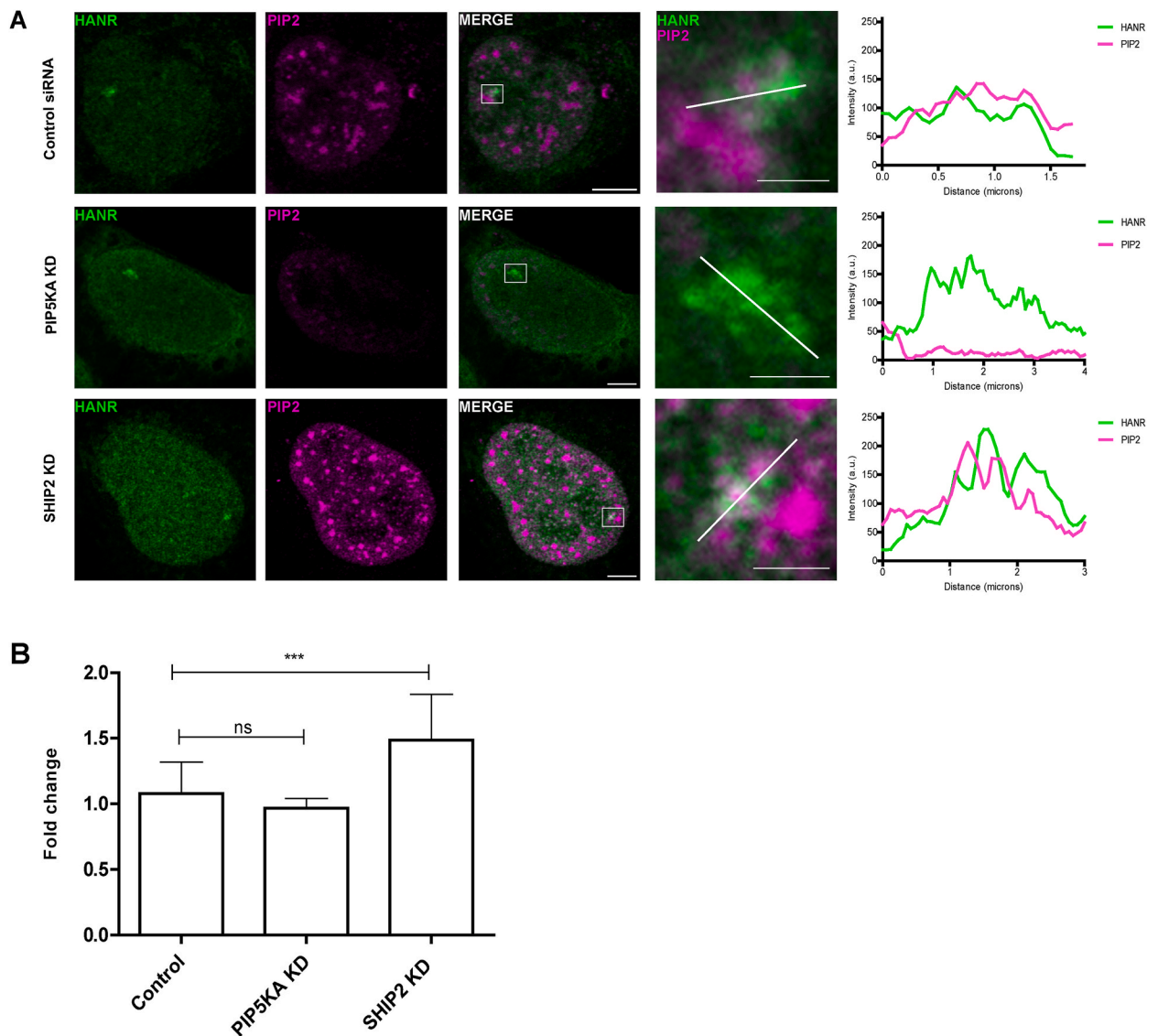
Fig. 7. *Manipulation with PIP2 levels leads to changes in the expression and localization of lncRNA HANR.* (A) Indirect immunostaining detecting lncRNA HANR is shown in a green channel with PIP2 in the magenta channel in cells treated either with control siRNA, siRNA against PIP5KA (downregulation of PIP2), and siRNA against SHIP2 (upregulation of PIP2). The scale bar represents 5 μm in the main images for all merged channels and 1 μm for the insets. B) RT-qPCR analysis of relative expression of lncRNA HANR in cells treated with control siRNA, PIP5KA KD and SHIP2 KD normalized to endogenous control. The results are related to three technical replicates for three biological replicates. Error bars represent mean SD. ns = non-significant P > 0.05, *** = P ≤ 0.001. (For interpretation of the references to colour in this figure legend, the reader is referred to the Web version of this article.)

3. Materials and methods

3.1. Cell culture

Human osteosarcoma U-2 OS cells (ATCC no. HTB96) and human adenocarcinoma HeLa cells (ATTC no. CRM-CCL-2) were grown in an incubator chamber at 37 °C with 5% CO_2 cultured in Dulbecco's modified Eagle's medium, high glucose (D6429, Merck, Darmstadt, Germany) supplemented with 10% Fetal bovine serum and gentamycin 40 μg/mL. HeLa cells were suspended in RPMI medium and supplemented with 5% FBS.

3.2. Nuclear RNA extraction

Nuclear RNA was extracted from a 500 mL HeLa cells spinning culture. The cells were harvested by centrifugation at 300g at 4 °C

for 1 min and washed three times with cold phosphate-buffered saline (PBS). The pellet was resuspended in 3 mL of ice-cold lysis buffer (50 mM Tris pH 7, 150 mM NaCl, 2 mM MgCl$_2$, 0.5% NP40, RNAse Block 1 in 100 μL) and spun at 1000 g at 4 °C for 10 min. The supernatant corresponding to the RNA cytoplasmic fraction was removed, and the pellet was resuspended in 3 mL of lysis buffer and spun at 1000 g at 4 °C for 1 min. The supernatant was discarded and 1.2 mL of lysis buffer was added to the pellet and transferred to a clean tube. Lysis buffer was added to the pellet, followed by the addition of 2.4 mL of Ribozol Extraction Reagent and 2.4 mL of chloroform, mixed with vortex and centrifuged at 12,000 g at 4 °C for 5 min. The upper aqueous phase was collected, and the RNA precipitated with 0.7 vol of isopropanol and centrifuged at 12,000 g at 4 °C for 15 min. After removing the solvent, the pellet was washed with 80% ethanol, air dried, and resuspended in DNA/RNAse-free water.

3.3. RNA binding protocol

For the RNA-PIP2 binding analysis, pull-down assays were conducted using agarose beads coated with lipids, as well as control beads without lipids. A pre-clearing step was performed where 200 μg of RNA was incubated with 100 μL of control beads and 1 μL of RNAse Block (Agilent Technologies) for 5 min. Following this, 100 μL of lipid-coated beads were prewashed with RNAse-free PBS, transferred to a clean tube, and precleared RNA was added. The samples were incubated for 30 min at 4 °C with gentle rotation. This process was carried out for lipid-coated beads and their corresponding controls without lipids. After incubation, the tubes were centrifuged at 1000 g for 1 min to remove unbound RNA. The beads were washed three times with 500 μL of RNAse-free PBS, with centrifugation repeated after each wash to ensure the beads remained intact during tube transfers.

For RNA extraction from the bound beads, 100 μL of RNAse-free PBS was added, followed by 200 μL of Ribozol and 200 μL of chloroform. The mixture was then centrifuged at 14,000 g for 10 min. The aqueous (upper) phase was carefully collected, and RNA was precipitated using 700 μL of isopropanol per 1 mL of the total volume. The RNA pellet was washed with ethanol and stored at −80 °C for further processing. This extracted RNA was subsequently used for sequencing.

All solutions designated as RNAse-free were treated with 1 μL/ml of RNAse Block. The beads used in the assay were Control beads (#P-B000), and PI(4,5)P2-coated beads (#P-B045a, also referred to as PIP2), both from Echelon Biosciences Inc.

3.4. Sequencing analysis

Sequencing was conducted for both Control (agarose beads without lipids) and PIP2 (agarose beads coated with PIP2 (PI(4,5)P2)) samples using Illumina 2 x 150 bp paired-end library sequencing. The sequencing libraries were prepared and processed by Novogene company. For the library construction, the ribosomal RNA was depleted using the NEB Ribo-ZeroTM kit, the RNA underwent reverse transcription into cDNA, and strand-specific libraries were prepared. The samples were sequenced using the platform Illumina Novaseq 6000 with a paired-end 150 bp read length. In this hypothesis-forming assay, we prioritized deeper sequencing over biological replicates.

The raw sequenced data underwent processing via the nf-core RNAseq pipeline version 3.8.1 (Ewels et al., 2020). Using the *Homo sapiens* (GRCh38) reference genome with annotation v107 from Ensembl (release 107, July 2022), the pipeline executed genome-guided data processing. QC procedures were applied, filtering out low-quality sequences (Phred score cutoff: 20) and adapter contaminants. The STAR aligner (version 2.7.10a), supporting splice-junction and fusion read detection, was selected for genome alignment. RSeQC (v5.0.1) was used to predict read distribution across different genome features. Transcript quantification was carried out using Salmon (v1.9.0), and the resulting count data were utilized for subsequent analyses. In the absence of replicates, differentially expressed transcripts (DETs) in the PIP2 sample were manually determined by comparing their expression to the Control sample, considering the fold change. A fold change value of 10 times higher was deemed significant for identifying DETs. To address the potential singular behavior of lowly expressed transcripts, a pseudo-count of 1 was added to all transcripts per kilobase million (TPM) values. Additionally, we examined the read distribution among the DETs using RSeQC (v5.0.1) for downstream analysis. To identify differentially expressed genes, mean fold change values were computed for all transcripts associated with each gene, treating this average as the fold change value for the respective gene. Similar to significant DETs, fold change values of 10 times higher were considered significant for identifying DEGs. The ncRNA-Seq raw data of all libraries were deposited in the National Center of Biotechnology Information (NCBI) with the BioProject accession: PRJNA937906. The accession numbers for BioSamples are SAMN33421421-Hs_INPUT, SAMN33421422-Hs_CONTROL, SAMN33421423-Hs_PIP2.

3.5. Gene set enrichment analysis and motif search

Functional enrichment of the differentially expressed genes was performed using Gene set enrichment analysis (GSEA), which utilizes the fold change values to rank genes. R software (version 4.3.2) in conjunction with the clusterProfiler package (v4.10.0) was employed for this purpose. The set of significantly up- and down-regulated DEGs was utilized for the over-representation analysis with all expressed genes in the PIP2 sample serving as the background (universe) for the analysis.

For motif enrichment analyses, we used the previously published data (Bayona-Hernandez et al., 2023). We employed the tool MEME from web-based MEME Suite Version 5.4.1 (https://meme-suite.org/meme/tools/meme).

For defining the PIP2 binding RNA motifs, we used the sequences of all overrepresented transcripts found in the PIP2-bound LIPRNAseq dataset and compared them to the sequences of the downregulated transcripts. We used a zero-order background model and searched for motifs with width between 6 and 200 on the RNAs. The PIP2 enriched motifs discovered by this setting are AU1 RNA motif - AUGUAAAAAAAAAAUUAAAGAAAAAAAAAAAAAAUAAAAA (width = 39, sites = 2488, p-value = 2×10^{-33}, E-value = $2 \times$

10^{-33}), and AU2 RNA motif - UUUUUCAAGAGUGAUAAAAAGUUUUUGGCCC (width = 31, sites = 2339, p-value = 2×10^{-17}, E-value = 2×10^{-17}).

To find a negative control motif that does not bind to PIP2 we used the list of all overrepresented transcripts found in empty beads (control) enriched RNA with the same setting conditions as above. This led to the discovery of GC-rich sequence CCGGGGCCUG-CUGGAGCCGGGGCUGCAGGCCCUCGCCCUCCGC (width = 43, sites = 4913, p-value = 2×10^{-138}, E-value = 2×10^{-138}), which was used as a negative control in our experiments.

3.6. HANR and AU1 and AU2 alignment

Clustal W was used for global sequence alignment of HANR and the motifs AU1 and AU2 with the default parameters.

3.7. In situ hybridization

U2-OS cells were grown on high-performance cover glasses of 12 mm diameter with a depth of 0.17 mm ± 0.005 mm and refractive index of 1.5255 ± 0.0015 (Marienfeld 0107222) for 24 h. The next day, cover glasses were washed with cold PBS, fixed with 4% formaldehyde in PBS for 15 min, and permeabilized with 0.5% Triton X-100 in PBS for 5 min. Cover glasses were than washed three times with PBS for a total of 30 min; cells were washed twice with Stellaris Buffer A (SMF-WA1-60, BiosearchTech, Hoddesdon, UK) for 5 min. Furthermore, cells were incubated in hybridization buffer (70% deionized formamide in 2 × SSC, 10 mM Tris-HCl, 2 mM MgCl$_2$, 0.5% Roche blocking reagent, 1 mg/mL yeast tRNA) for 16 h at 37 °C in a humidified chamber. After the hybridization, cells were washed with Stellaris Buffer A (SMF-WA1-60, BiosearchTech, Hoddesdon, UK) for 30 min at 37 °C, followed by one wash with Stellaris Buffer B (SMF-WB1-20 BiosearchTech, Hoddesdon, UK) for 5 min at room temperature and blocked with 3% bovine serum albumin (BSA) in PBS.

Probes were designed as reverse complementary sequences to target specific RNA nucleotide sequences for *in situ* hybridization. All probes were synthesized and labeled with biotin at the 5′ end. All probes were used in the final concentration of 50 μg/mL. We used the target sequence (5' → 3') for GC control: CCGGGGCCUGCUGGAGCCGGGGCUGCAGGCCCUCGCCCUCCGC. The AU1 complementary probe was designed against the target sequence: UUUUUAUUUUUUUUUUUUUCUUUAAUUUUUUUUUUUACAU. The AU2 complementary probe was designed targeting the following sequence: GGGCCAAAAACUUUUUAUCACUCUUGAAAAA. The AU1 and AU2 probes were used as templates to generate scrambled probes to determine the specificity of hybridization — the scrambled version of the AU1 probe UUUUUUUAUUUUUUCUUAAUUUUUAUUUACAUUUUUUU and the scrambled version of the AU2 probe UAAG-GAAACCUGUAUUCGUUAAAUAACACUC. The HANR probe was generated using the sequence of *Homo sapiens* ribosomal protein L13a pseudogene 20 (RPL13AP20), non-coding RNA (Sequence ID: AC007688.15; NM_012423) where we selected the following region for specific probe design: UUCAUGAGGCUAUGGAAACAGGCCGAGAAGAACGUGGAG.

After the blocking step, incubation with primary antibodies was performed for 1 h at room temperature. The cells were then washed three times with PBS for 30 min and incubated with secondary antibodies [anti-Mouse AlexaFluo 488 (1696430), anti-Rabbit Alex-aFluo 568 (1386541) and anti-Mouse Alexa 568 (1786285), Invitrogen, Waltham, Massachusetts, USA] in dark for 1 h. The cells were washed with PBS for 15 min, incubated with DAPI for 2 min, and then washed twice for 10 min. At last, upon air-drying, the cover glasses were mounted using AD-MOUNT (ADM-005, Life M s.r.o, Prague, Czechia).

We used the following primary antibodies for immunofluorescent detection of target molecules according to the manufacturer's instructions and concentration recomendations: Anti-Biotin (200-002-12, Jackson ImmunoResearch, Cambridge, UK); Anti-Biotin (ab53494, Abcam, Cambridge, UK); Anti-PIP2 (AB010220-28, Echelon Biosciences, Salt Lake City, Utah, USA); Anti-MED1 (HPA052818, Sigma-Aldrich, St. Louis, Missouri, USA); Anti-SON (AB121759, Abcam, Cambridge, United Kingdom); Anti-SFPQ (AB177149, Abcam, Cambridge, United Kingdom); Anti-PML (ABD-030, Jena Bioscience, Jena, Germany); Anti-Coilin (sc-32860, Santa Cruz Biotechnology, Dallas, Texas, USA); Anti-Myosin1 (HPA001768, Sigma-Aldrich, St. Louis, Missouri, USA); Anti-Nucleolin (AB22758, Abcam, Cambridge, United Kingdom); Anti-RNA Polymerase I (PAF53) was kindly provided by Ingrid Grummt, Anti-RNA Polymerase II (ab210527, Abcam, Cambridge, United Kingdom); Anti-RAD51 (ab63801, Abcam, Cambridge, United Kingdom); and Anti-Fibrillarin (2639S, Cell Signaling Technology, Danvers, Massachusetts, USA).

Secondary antibodies used for immunofluorescence at 1:400 dilution were: Goat anti-Mouse IgM (Heavy chain) Cross-Adsorbed, Alexa Fluor 568, A-21043 (Invitrogen, MA, USA); Goat anti-Mouse IgG (H + L) Highly Cross-Adsorbed, Alexa Fluor 488, A-11029 (Invitrogen, MA, USA); Goat anti-Mouse IgG (H + L) Highly Cross-Adsorbed, Alexa Fluor 568, A-11031 (Invitrogen, MA, USA); Goat anti-Rabbit IgG (H + L) Cross-Adsorbed, Alexa Fluor 568, A-11011 (Invitrogen, MA, USA); and Goat anti-Rabbit IgG (H + L) Highly Cross-Adsorbed, Alexa Fluor 488, A-11034 (Invitrogen, MA, USA).

Images were then acquired using confocal microscopes Leica TCS SP8 and Leica STELLARIS 8 FALCON (Leica Mikrosysteme Vertrieb GmbH, Wetzlar, Germany) with oil objective ×63 NA 1,4. DeltaVision OMX^T V4 SIM with oil objective ×63 (0,1516). All images presented in the paper are the representative images for the given staining and each experiment was performed in at least three independent replicates.

3.8. Knockdown of PIP2-regulating enzymes

U2-OS cells were grown for 24 h before transfection using MISSION esiRNA PIP5K1A (EHU114801, Sigma-Aldrich, MO, USA) or MISSION esiRNA SHIP2 (EHU081051, Sigma-Aldrich, MO, USA) and Lipofectamine RNA iMAX (13778075, Invitrogen, MA, USA) according to the manufacturer's instructions. MISSION siRNA Universal Negative Control #1 (SIC001, Sigma-Aldrich, MO, USA) was

used as the negative control. The subsequent analysis of transiently transfected cells was performed 24 h after the transfection. The knockdown was repeated in three independent experiments with similar results.

3.9. Real-time quantitative PCR

U2-OS cells were collected using TRIzol (BCCF 2003, Sigma, MO, USA) per the manufacturer's protocol. Shortly, the lysate was centrifuged for 1 min, 12,000 g at 4 °C, and the supernatant was collected and placed for 5 min at room temperature. After adding chloroform, the samples were mixed vigorously and placed for 5 min at room temperature. A centrifugation of 15 min, 12,000 g at 4 °C, was performed, and the upper aqueous phase was transferred to a new tube in which 2.5 vol of 100 % ethanol were added. The tubes were then transferred for at least 30 min at −20 °C. The tubes were centrifuged for 30 min, 13,000 g at 4 °C, and, after removal of the supernatant, 80 % ethanol freshly made was added and centrifuged for 30 min, 13,000 g at 4 °C. The supernatant was removed, and the pellet air dried before adding DNase/RNase-free water and quantified at Nanodrop.

One μg of isolated RNA for each condition was used for the reverse transcriptase reaction, for which we used RevertAid Reverse Transcriptase (EP0441, ThermoFisher Scientific, MA, USA). The program setting was as follows: 25 °C for 10 min, 42 °C for 1 h, and 70 °C for 10 min.

The setting of RT-qPCR was set up to 95 °C for 10 s, 95 °C for 15 s, 58 °C for 15 s, and 72 °C for 25 s for 50 cycles. The RT-qPCR was performed using LightCycler 480 SYBR Green I Master (04887352001, Roche, Switzerland). Three technical replicates for each of the three biological replicates were used for the analysis.

The primers used for RT-qPCR experiments for HANR expression were designed using the sequence for *Homo sapiens* ribosomal protein L13a pseudogene 20 (RPL13AP20) (NM_012423): Fwd: CTCAAGGTGTTTGACGGCATCC; Rev: TACTTCCAGCCAACCTCGT-GAG. For expression of the housekeeping gene, we used primers detecting *Homo sapiens* ACTB (NM_001101): Fwd: AGGCAC-CAGGGCGTGAT; Rev: TCGCCCACATAGGAATCCTT.

Average ct values were calculated from each experiment, and sample values were normalized to the housekeeping gene *ACTB* using the ΔΔCt method.

4. Discussion

Cancer prognostic markers, including the expression of specific genes, the accumulation of specific proteins to particular compartments, or biochemical changes, are biological indicators that provide information about the likely course and outcome of cancer in the individual. Oncogenic super-enhancers, the PNC, and lncRNA HANR have all been identified as prognostic markers, present in the majority of cancer cell lines and tested tumors. Their presence is associated with poor survival outcomes and high tumorigenic potential (Badowski et al., 2022; Beylerli et al., 2022; Qian et al., 2020; Hu et al., 2022). However, these elements have never been linked together and have only been studied as separate entities. This is understandable in the case of the lncRNA HANR, as it was discovered recently, and minimal literature is available describing its function (Xiao et al., 2017; Xu et al., 2020). A direct connection between the PNC and oncogenic super-enhancers is also absent in the literature, likely due to the distinct biological roles described for each. While super-enhancers are associated with Pol II transcription of specific oncogenes (Jia et al., 2020; Barshad et al., 2023; Qian et al., 2023; Sengupta et al., 2017), the PNC, located near the nucleolus, is involved in ribosome biogenesis, mRNA splicing, and possibly *Pol*I transcription by sequestering proteins important for rRNA synthesis (Frankowski et al., 2022; Mattick et al., 2023).

Here, we demonstrate that super-enhancers and the PNC colocalize with PIP2 and lncRNA HANR, possibly forming a functionally interconnected structure. We propose that the super-enhancers and perinucleolar compartment are, in fact, part of the same structure. This is interesting from the perspective of chromosomal organization, as it raises a question about the need for the spatial distribution of the super-enhancers in close vicinity to the nucleolus. Although the precise reason why oncogenic super-enhancers are close to nucleoli requires experimental elucidation, one possible explanation is that mutual communication between the two transcription machineries may ensure a coordinated response to cellular needs and environmental changes.

Oncogenic super-enhancers drive the overexpression of proteins that regulate cell proliferation, associated with increased ribosome biogenesis to supply the necessary proteins for growing cells (See et al., 2022). Thus, the proximity of the *Pol*I and Pol II machinery could serve as a regulatory hub, coordinating the functions of both systems. This coordination might occur through local epigenetic modifications that create a favorable transcriptional environment for both polymerases or through the shared use of transcription factors, regulatory protein complexes, or other resources such as actin and myosin, c-Myc, Reb1, or TBP (Zhang et al., 2017). PIP2 itself has been shown to have a role in *Pol*I and Pol II transcription, as well as mRNA splicing (Sobol et al., 2014, 2018; Yildirim et al., 2013), and could therefore serve as a common link between the two transcription machineries. However, its depletion does not lead to the dissociation of the PNC and loss of lncRNA HANR, suggesting that PIP2 may have a supporting rather than structural function. Another explanation may be that enzymatic manipulation of PIP2 levels is not efficient enough to affect the PIP2 levels globally. It rather affects the PIP2 functions in isolated parts of the nucleus.

In summary, this study investigated the link between PIP2, RNA, and various nuclear proteins that produce phase-separated structures. Employing the LIPRNAseq technique, we identified lncRNA HANR interacting with PIP2 in the PNC, together with oncogenic super-enhancer markers, suggesting that the PNC and oncogenic super-enhancers are part of the same structure. Therefore, using any of the three cancer prognosis markers – lncRNA HANR, perinucleolar compartment, or oncogenic super-enhancers could have the same diagnostic significance in patient prognosis. Finally, understanding the relationship between lipid metabolism and lncRNAs and their specific roles in the phase separation of subnuclear compartments, as well as understanding cancer behavior through the prognostic markers, can lead to tailored treatment, improvement of patient outcomes, and personalized cancer

management.

CRediT authorship contribution statement

Ana Miladinović: Conceptualization, Investigation, Methodology, Validation, Visualization, Writing – original draft, Writing – review & editing. **Ludovica Antiga:** Conceptualization, Investigation, Methodology, Validation, Visualization, Writing – original draft, Writing – review & editing. **Tomáš Venit:** Conceptualization, Investigation, Methodology, Supervision, Validation, Visualization, Writing – original draft, Writing – review & editing. **Andrea Bayona-Hernandez:** Formal analysis, Investigation, Methodology, Validation, Writing – review & editing. **Jakub Červenka:** Conceptualization, Formal analysis, Methodology, Writing – review & editing. **Rajendra Kumar Labala:** Data curation, Formal analysis, Methodology, Visualization, Writing – review & editing. **Michal Kolář:** Conceptualization, Data curation, Formal analysis, Funding acquisition, Writing – review & editing. **Enrique Castaño:** Conceptualization, Investigation, Methodology, Writing – review & editing. **Martin Sztacho:** Conceptualization, Funding acquisition, Methodology, Supervision, Writing – review & editing. **Pavel Hozak:** Conceptualization, Funding acquisition, Methodology, Project administration, Resources, Supervision, Validation, Writing – review & editing.

Declaration of competing interest

The authors declare that they have no known competing financial interests or personal relationships that could have appeared to influence the work reported in this paper.

Acknowledgment

Appendix A. Supplementary data

Supplementary data to this article can be found online at https://doi.org/10.1016/j.jbior.2024.101069 and https://www.ncbi.nlm.nih.gov/bioproject/PRJNA937906

Data availability

Data will be made available on request.

References

Adeel, M.M., et al., 2021. Structural variations of the 3D genome architecture in cervical cancer development. Front. Cell Dev. Biol. 9.

Ayupe, A.C., et al., 2015. Global analysis of biogenesis, stability and sub-cellular localization of lncRNAs mapping to intragenic regions of the human genome. RNA Biol. 12 (8), 877–892.

Bacabac, M., Xu, W., 2023a. Oncogenic super-enhancers in cancer: mechanisms and therapeutic targets. Cancer Metastasis Rev. 42 (2), 471–480.

Bacabac, M., Xu, W., 2023b. Oncogenic super-enhancers in cancer: mechanisms and therapeutic targets. Cancer Metastasis Rev. 42 (2), 471–480.

Badowski, C., He, B., Garmire, L.X., 2022. Blood-derived lncRNAs as biomarkers for cancer diagnosis: the Good, the Bad and the Beauty. npj Precis. Oncol. 6 (1), 40.

Balaban, C., et al., 2021. The F-Actin-Binding MPRIP forms phase-separated condensates and associates with PI(4,5)P2 and active RNA polymerase II in the cell nucleus. Cells 10 (4).

Balaban, C., et al., 2023. PIP2-Effector protein MPRIP regulates RNA polymerase II condensation and transcription. Biomolecules 13 (3).

Barshad, G., et al., 2023. RNA polymerase II dynamics shape enhancer-promoter interactions. Nat. Genet. 55 (8), 1370–1380.

Bayona-Hernandez, A., et al., 2023. LIPRNAseq: a method to discover lipid interacting RNAs by sequencing. Mol. Biol. Rep. 50 (8), 6619–6626.

Beylerli, O., et al., 2022. Long noncoding RNAs as promising biomarkers in cancer. Non-coding RNA Research 7 (2), 66–70.

Blayney, J.W., et al., 2023. Super-enhancers include classical enhancers and facilitators to fully activate gene expression. Cell 186 (26), 5826–5839.e18.

Boija, A., et al., 2018. Transcription factors activate genes through the phase-separation capacity of their activation domains. Cell 175 (7), 1842–1855 e16.

Casalin, I., et al., 2024. Nuclear phospholipids and signaling: an update of the story. Cells 13 (8).

Castano, E., et al., 2019. Nuclear phosphoinositides-versatile regulators of genome functions. Cells 8 (7).

Cavellan, E., et al., 2006. The WSTF-SNF2h chromatin remodeling complex interacts with several nuclear proteins in transcription. J. Biol. Chem. 281 (24), 16264–16271.

Das, N.D., et al., 2023. Defining super-enhancers by highly ranked histone H4 multi-acetylation levels identifies transcription factors associated with glioblastoma stem-like properties. BMC Genom. 24 (1), 574.

Debek, S., Juszczynski, P., 2022. Super enhancers as master gene regulators in the pathogenesis of hematologic malignancies. Biochim. Biophys. Acta Rev. Canc 1877 (2), 188697.

Deleris, P., et al., 2003. SHIP-2 and PTEN are expressed and active in vascular smooth muscle cell nuclei, but only SHIP-2 is associated with nuclear speckles. J. Biol. Chem. 278 (40), 38884–38891.

Derrien, T., et al., 2012. The GENCODE v7 catalog of human long noncoding RNAs: analysis of their gene structure, evolution, and expression. Genome Res. 22 (9), 1775–1789.

Dumelie, J.G., et al., 2024. Biomolecular condensates create phospholipid-enriched microenvironments. Nat. Chem. Biol. 20 (3), 302–313.

Eidelman, Y.A., et al., 2017. Nuclear 3D organization and radiosensitivity. J. Phys. Conf. 784.

Ewels, P.A., et al., 2020. The nf-core framework for community-curated bioinformatics pipelines. Nat. Biotechnol. 38 (3), 276–278.

Frankowski, K.J., et al., 2022. Discovery and optimization of pyrrolopyrimidine derivatives as selective disruptors of the perinucleolar compartment, a marker of tumor progression toward metastasis. J. Med. Chem. 65 (12), 8303–8331.

Hazan, I., et al., 2019. Activation of oncogenic super-enhancers is coupled with DNA repair by RAD51. Cell Rep. 29 (3), 560–572 e4.

Hirose, T., et al., 2014. NEAT1 long noncoding RNA regulates transcription via protein sequestration within subnuclear bodies. Mol. Biol. Cell 25 (1), 169–183.

Hirose, T., Yamazaki, T., Nakagawa, S., 2019. Molecular anatomy of the architectural NEAT1 noncoding RNA: the domains, interactors, and biogenesis pathway required to build phase-separated nuclear paraspeckles. WIREs RNA 10 (6), e1545.

Hnisz, D., et al., 2013. Super-enhancers in the control of cell identity and disease. Cell 155 (4), 934–947.

Hnisz, D., et al., 2017. A phase separation model for transcriptional control. Cell 169 (1), 13–23.

Hoboth P, Šebesta O, Sztacho M, Castano E, Hozák P. Dual-color dSTORM imaging and ThunderSTORM image reconstruction and analysis to study the spatial organization of the nuclear phosphatidylinositol phosphates. MethodsX. 2021 May 1;8:101372. doi: 10.1016/j.mex.2021.101372. PMID: 34430268; PMCID: PMC8374474.

Hoboth, P., et al., 2023. Quantitative super-resolution microscopy reveals the differences in the nanoscale distribution of nuclear phosphatidylinositol 4,5-bisphosphate in human healthy skin and skin warts. Front. Cell Dev. Biol. 11, 1217637.

Hoboth, P., Sztacho, M., Hozak, P., 2024. Nuclear patterns of phosphatidylinositol 4,5- and 3,4-bisphosphate revealed by super-resolution microscopy differ between the consecutive stages of RNA polymerase II transcription. FEBS J. 291 (19), 4240–4264.

Hu, Q., et al., 2022. LncRNA in tumorigenesis of non-small-cell lung cancer: from bench to bedside. Cell Death Dis. 8 (1), 359.

Iyer, M.K., et al., 2015. The landscape of long noncoding RNAs in the human transcriptome. Nat. Genet. 47 (3), 199–208.

Jia, Y., Chng, W.J., Zhou, J., 2019. Super-enhancers: critical roles and therapeutic targets in hematologic malignancies. J. Hematol. Oncol. 12 (1), 77.

Jia, Q., et al., 2020. Oncogenic super-enhancer formation in tumorigenesis and its molecular mechanisms. Exp. Mol. Med. 52 (5), 713–723.

Kim, T., et al., 2022. Comparative characterization of 3D chromatin organization in triple-negative breast cancers. Exp. Mol. Med. 54 (5), 585–600.

Lewis, A.E., et al., 2011. Identification of nuclear phosphatidylinositol 4,5-bisphosphate-interacting proteins by neomycin extraction. Mol. Cell. Proteomics 10 (2), S1–S15.

Li, R.-H., et al., 2021. A phosphatidic acid-binding lncRNA SNHG9 facilitates LATS1 liquid–liquid phase separation to promote oncogenic YAP signaling. Cell Res. 31 (10), 1088–1105.

Lin, A., et al., 2017. The LINK-A lncRNA interacts with PtdIns(3,4,5)P(3) to hyperactivate AKT and confer resistance to AKT inhibitors. Nat. Cell Biol. 19 (3), 238–251.

Liu, S., et al., 2024. Effects of super-enhancers in cancer metastasis: mechanisms and therapeutic targets. Mol. Cancer 23 (1), 122.

Lundquist, M.R., et al., 2018. Phosphatidylinositol-5-Phosphate 4-kinases regulate cellular lipid metabolism by facilitating autophagy. Mol. Cell 70 (3), 531–544 e9.

Luo, J., et al., 2021. LncRNAs: architectural scaffolds or more potential roles in phase separation. Front. Genet. 12, 626234.

Makeyev, E.V., Huang, S., 2024. The perinucleolar compartment: structure, function, and utility in anti-cancer drug development. Nucleus 15 (1).

Mao, Y.S., et al., 2010. Direct visualization of the co-transcriptional assembly of a nuclear body by noncoding RNAs. Nat. Cell Biol. 13 (1), 95–101.

Mattick, J.S., et al., 2023. Long non-coding RNAs: definitions, functions, challenges and recommendations. Nat. Rev. Mol. Cell Biol. 24 (6), 430–447.

Norton, J.T., et al., 2009. The perinucleolar compartment is directly associated with DNA. J. Biol. Chem. 284 (7), 4090–4101.

Norton, J.T., Huang, S., 2013. The perinucleolar compartment: RNA metabolism and cancer. Cancer Treat Res. 158, 139–152.

Obrdlik, A., et al., 2010. Nuclear myosin 1 is in complex with mature rRNA transcripts and associates with the nuclear pore basket. Faseb. J. 24 (1), 146–157.

Owusu Obeng, E., et al., 2020. Phosphoinositide-dependent signaling in cancer: a focus on phospholipase C isozymes. Int. J. Mol. Sci. 21 (7).

Percipalle, P., et al., 2006. The chromatin remodelling complex WSTF-SNF2h interacts with nuclear myosin 1 and has a role in RNA polymerase I transcription. EMBO Rep. 7 (5), 525–530.

Pestic-Dragovich, L., et al., 2000. A myosin I isoform in the nucleus. Science 290 (5490), 337–341.

Philimonenko, V.V., et al., 2004. Nuclear actin and myosin I are required for RNA polymerase I transcription. Nat. Cell Biol. 6 (12), 1165–1172.

Pisani, G., Baron, B., 2019. Nuclear paraspeckles function in mediating gene regulatory and apoptotic pathways. Noncoding RNA Res 4 (4), 128–134.

Pollock, C., Huang, S., 2010. The perinucleolar compartment. Cold Spring Harbor Perspect. Biol. 2 (2), a000679.

Posor, Y., Jang, W., Haucke, V., 2022. Phosphoinositides as membrane organizers. Nat. Rev. Mol. Cell Biol. 23 (12), 797–816.

Qian, Y., Shi, L., Luo, Z., 2020. Long non-coding RNAs in cancer: implications for diagnosis, prognosis, and therapy. Front. Med. 7, 612393.

Qian, H., et al., 2023. Super-enhancers and the super-enhancer reader BRD4: tumorigenic factors and therapeutic targets. Cell Death Dis. 9 (1), 470.

Ratti, S., et al., 2021. Modulating phosphoinositide profiles as a roadmap for treatment in acute myeloid leukemia. Front. Oncol. 11, 678824.

Sabari, B.R., et al., 2018. Coactivator condensation at super-enhancers links phase separation and gene control. Science 361 (6400).

See, Y.X., Chen, K., Fullwood, M.J., 2022. MYC overexpression leads to increased chromatin interactions at super-enhancers and MYC binding sites. Genome Res. 32 (4), 629–642.

Sengupta, S., George, R.E., 2017. Super-enhancer-driven transcriptional dependencies in cancer. Trends Cancer 3 (4), 269–281.

Shadrina, O.A., et al., 2022. SFPQ and NONO proteins and long non-coding NEAT1 RNA: cellular functions and role in the HIV-1 Life cycle. Mol. Biol. 56 (2), 196–209.

Shevtsov, S.P., Dundr, M., 2011. Nucleation of nuclear bodies by RNA. Nat. Cell Biol. 13 (2), 167–173.

Sobol, M., et al., 2014. UBF complexes with phosphatidylinositol 4,5-bisphosphate in nucleolar organizer regions regardless of ongoing RNA polymerase I activity. Nucleus 4 (6), 478–486.

Sobol, M., et al., 2018. Nuclear phosphatidylinositol 4,5-bisphosphate islets contribute to efficient RNA polymerase II-dependent transcription. J. Cell Sci. 131 (8).

Somasundaram, K., et al., 2022. LncRNAs divide and rule: the master regulators of phase separation. Front. Genet. 13, 930792.

Sztacho, M., et al., 2019. Nuclear phosphoinositides and phase separation: important players in nuclear compartmentalization. Adv Biol Regul 71, 111–117.

Sztacho, M., et al., 2021. Limited proteolysis-coupled mass spectrometry identifies phosphatidylinositol 4,5-bisphosphate effectors in human nuclear proteome. Cells 10 (1).

Sztacho, M, Červenka, J, Šalovská, B, Antiga, L, Hoboth, P, Hozák, P, 2024 Dec 2. The RNA-dependent association of phosphatidylinositol 4,5-bisphosphate with intrinsically disordered proteins contribute to nuclear compartmentalization. PLoS Genet. 20 (12), e1011462. https://doi.org/10.1371/journal.pgen.1011462. Epub ahead of print. PMID: 39621780.

Tang, Z., et al., 2015. CTCF-mediated human 3D genome architecture reveals chromatin topology for transcription. Cell 163 (7), 1611–1627.

Tong, C., Yin, Y., 2021. Localization of RNAs in the nucleus: cis- and trans- regulation. RNA Biol. 18 (12), 2073–2086.

Tong, X., et al., 2022. Liquid-liquid phase separation in tumor biology. Signal Transduct. Targeted Ther. 7 (1), 221.

Villar, D., et al., 2015. Enhancer evolution across 20 mammalian species. Cell 160 (3), 554–566.

Wang, X., Cairns, M.J., Yan, J., 2019. Super-enhancers in transcriptional regulation and genome organization. Nucleic Acids Res. 47 (22), 11481–11496.

Wang, Y., Chen, L.-L., 2020. Organization and function of paraspeckles. Essays Biochem. 64 (6), 875–882.

Wen, T., et al., 2023. Regulation of phosphoinositide signaling by scaffolds at cytoplasmic membranes. Biomolecules 13 (9).

Whyte, W.A., et al., 2013. Master transcription factors and mediator establish super-enhancers at key cell identity genes. Cell 153 (2), 307–319.

Xiao, J., et al., 2017. LncRNA HANR promotes tumorigenesis and increase of chemoresistance in hepatocellular carcinoma. Cell. Physiol. Biochem. 43 (5), 1926–1938.

Xu, M., et al., 2020. Long non-coding RNA HANR as a biomarker for the diagnosis and prognosis of colorectal cancer. Medicine (Baltim.) 99 (7), e19066.

Yap, K., et al., 2018. A short tandem repeat-enriched RNA assembles a nuclear compartment to control alternative splicing and promote cell survival. Mol. Cell 72 (3), 525–540 e13.

Yildirim, S., et al., 2013. Involvement of phosphatidylinositol 4,5-bisphosphate in RNA polymerase I transcription. J. Cell Sci. 126 (Pt 12), 2730–2739.

Zaghlool, A., et al., 2021. Characterization of the nuclear and cytosolic transcriptomes in human brain tissue reveals new insights into the subcellular distribution of RNA transcripts. Sci. Rep. 11 (1), 4076.

Zhang, Y., Najmi, S.M., Schneider, D.A., 2017. Transcription factors that influence RNA polymerases I and II: to what extent is mechanism of action conserved? Biochim Biophys Acta Gene Regul Mech 1860 (2), 246–255.